AIAA 79-1758R

Optimization of Earth Sensor Thresholding Techniques

R.H. Anderson,* C.I. Heiling,† A.Y. Okomoto,‡ and H.E. Zimmerman§
Lockheed Missiles & Space Company, Inc., Sunnyvale, Calif.

A high-accuracy synchronous-orbit Earth sensor with large off-axis pointing capability has been developed. For this new design, the sensor operation was analyzed, varying each parameter as part of the optimization. The analysis simulated operation from the Earth model through sensor output, with the optimization accounting for Earth radiance variations (latitude and season), scan geometry, and all electronic parameters. The effect on the tradeoffs between system noise and seasonal radiance errors for each parameter is discussed. The final results, verified by test, are presented.

Nomenclature

$B(\lambda,i)$	= blackbody radiation of the ith segment
dV/dt	= slope at threshold
G	= a constant
K	= signal slope
n	= number of segments
NEB	= noise equivalent bandwidth
O	= (possible) boundary conditions, i.e., clouds
V_H	= hold voltage
V_p	= peak output voltage
V_{th}	= threshold voltage
λ	= wavelength
$\epsilon(\lambda,i)$	= emissivity of the segment
τ	= fixed time delay
$\tau(\lambda,i)$	= transmissivity of the segment
τ_D	= detector time constant = 2 ms (80 Hz)
τ_1	= high-frequency filter = 0 (for computer simulation)
τ_2	= 5.1 s
τ_3	= τ_5, two poles determining upper cutoff frequency
τ_4	= 3.3 s
τ_6	= one pole determining lower cutoff frequency
τ_7	= ¼ τ_D, treble boost (frequency compensation at 80 Hz)

Introduction

IN optimizing a scanning Earth sensor design to minimize the effects of the north-south radiance gradients as seen from synchronous orbit, it is necessary to look at how each parameter contributes to the system performance. The sensor being designed was based on a previously qualified system.[1] Therefore, it was decided to make no changes to the optics, spectral band, detectors, and scanning mirror. As a result, radiance gathered, field-of-view, and scanning frequency were considered fixed. The electronic parameters in the transfer function, thresholding techniques, and computation algorithm were considered as variables to be adjusted in the optimization, and the variable inputs were Earth radiance (latitude and season), satellite altitude, and satellite attitude.

The Problem

The satellite system consists of two identical sensors, one aligned east-west and the other north-south. The resulting scan pattern is illustrated in Fig. 1.

Presented as Paper 79-1758 at the AIAA Guidance and Control Conference, Boulder, Colo., Aug. 6-8, 1979; submitted Oct. 30, 1979; revision received July 28, 1980.

*Project Leader, Sensor Technology, Space Systems Div.
†Research Specialist, Guidance and Control, Space Systems Div.
‡Research Specialist, Sensor Technology, Space Systems Div.
§Sr. Staff Engineer, Program Engineer, Space Systems Div.

The Earth's radiance, in the sensors' 14.1-15.8 spectral band, varies primarily with latitude and season. The seasonal changes are due to the sun's position with respect to the Earth, causing the greatest radiance from the polar summer conditions and the least from the polar winter conditions. The extreme months are January and July with the southern fluxuations slightly greater than those in the north. This radiance variation is accentuated by the field-of-view moving rapidly through the polar latitudes as compared to the equatorial latitudes as illustrated in Fig. 2.

The resulting input to the sensor with a worst-case radiance condition convolved by the field-of-view is also illustrated in Fig. 2. The basic problem, then, can be stated as: "Find the geometric centroid of the Earth as it moves about (in size and position) in the scan pattern and its radiance varies with season and latitude."

The Tools

To perform the analyses required for the optimization, several computer programs were required. A summary of their capability follows:

Earth Radiance

This program builds a model of the Earth's atmospheric radiance as a function of temperature, pressure, altitude, and spectral band.

The primary atmospheric data used to build the current model is derived from measurements by the Selective Chopper Radiometer (SCR) flown on NIMBUS IV and reported in Refs. 2-4. This data, augmented by data from Refs. 5 and 6 is formed into a composite model of the atmosphere.

To systematize the calculation of Earth radiance for reasonable computer application, it is convenient to consider the Earth's atmosphere as a series of equally spaced concentric shells. The above composite atmospheric data is converted to a shell model by use of logarithmic interpolation and basic equations of atmospheric physics.

In preparation for the calculation of radiance, it is necessary to determine the envelope of possible optical paths. Earth radiance is assumed relatively insensitive to longitude, hence only two quantities are required to specify a line of sight—a tangent altitude and a zenith angle at that altitude. Given the concentric shell model, each optical path is segmented, and the total radiance sensed is the integrated effect of all radiating molecules in that optical path. Radiance is calculated as

$$N(\lambda) = B(\lambda,0)\epsilon(\lambda,0)\tau(\lambda,0) + B(\lambda,i)\epsilon(\lambda,i)\tau(\lambda,i)$$

Transmissions for CO_2 and O_3 are calculated using the Elsasser band model and H_2O transmissions are calculated using the Goody model.

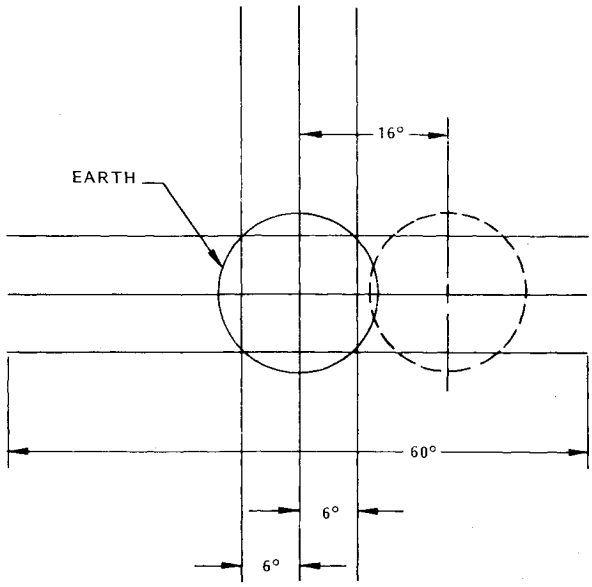

Fig. 1 Scan pattern.

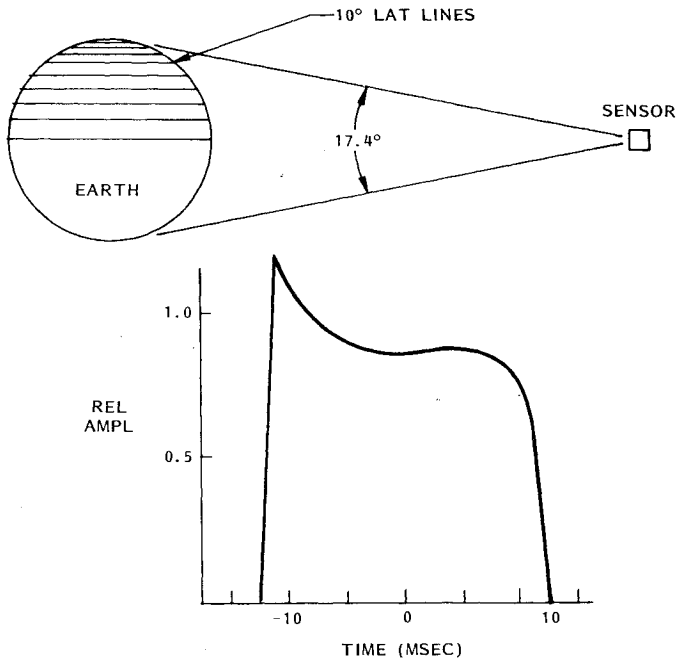

Fig. 2 Scan across the Earth and radiance input.

In order to build a profile for a given latitude, 43 paths are computed: eight are paths that intercept the ground at various zenith angles, and the remainder are tangent heights up to 80 km. This process is repeated for 19 latitudes from north to south and results in a complete Earth radiance model for a given day. Data is available for 22 days spanning the entire seasonal cycle.

Geometric Input

The output of program 1 is then fed into the convolution program which computes the radiance seen by a specific aperture scanning from a position defined by vehicle attitude and altitude. It does this by coordinating the field of view and integrating over both axes as the field-of-view moves along the scan plane intersection with the Earth. The output is then saved for use by the following program.

Transfer Function Response and Thresholding

This program processes an arbitrary input through a series of electronic amplifiers, whose transfer function modifies the

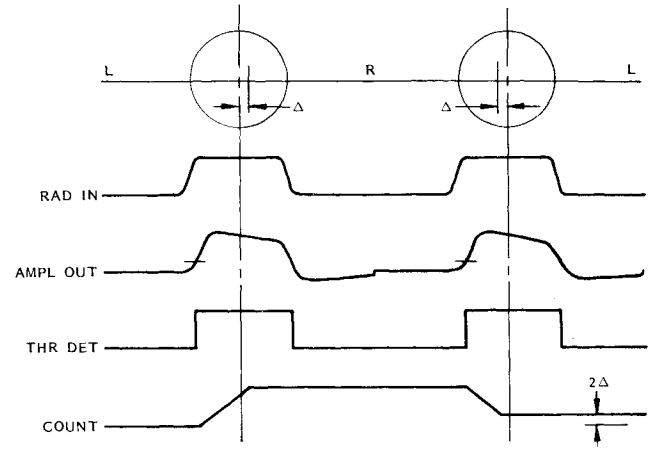

Fig. 3 Signal processing algorithm.

wave into a signal that is thresholded to determine the Earth's horizon. This is accomplished by taking the Fourier transform of the input time function and multiplying it by the Fourier transform of the transfer function to obtain the frequency domain response. An inverse Fourier transform is then used to construct the time domain output wave. Thresholding is accomplished using an iterative solution of the thresholding algorithm presented in a later section. Sensed vehicle attitude is derived from threshold times of a complete bidirectional scan and compared with the known vehicle input attitude to determine sensor error.

These programs can be worked sequentially and in an iterative fashion to observe the final effect of each parameter. Intermediate results are highly visible, as the programs provide large amounts of output in both numerical and plot forms.

Processing Algorithm

The Earth sensor scanning mirror system contains an optical encoder which provides a pulse for each 0.01 deg of field-of-view motion and a center reference pulse when the field-of-view is pointing straight ahead. The position of the Earth is calculated by comparing the angle from the horizon to mirror center to the angle from the opposite horizon to mirror center. This is done independently for any field-of-view crossing the Earth. The calculation is performed for each direction of scan and several scans averaged for each output update.

The primary source of error is caused by the signal represented in Fig. 2. The radiance gradient across the Earth biases the space to Earth horizon crossing. This occurs in a different manner depending on the direction of scan, compounding the problem. Preliminary analyses were made which showed the best thresholding technique to be a slope-sensitive system using only the space to Earth crossings of the field-of-view. The results of this analysis are shown in Table 1.

Using this algorithm, only half of the available data is used so there is a $\sqrt{2}$ increase in the noise-equivalent angle of the output. The Earth sensor signal processing is then as illustrated in Fig. 3.

Thresholding Technique

The slope-sensitive thresholding technique is illustrated in Fig. 4. V_{th} is determined by dividing V_H by G with a resistor pair. V_H is determined by charging a capacitor for a fixed time τ after threshold has occurred and then holding that voltage. As a result, it can be seen that V_{th} is proportional to the slope K of the signal, where τ and G are circuit parameters to be optimized.

Transfer Function

The bandpass of the amplifiers determine the amount of noise it passes and the response to the incoming Earth signal.

This bandpass is represented by the transfer function shown in Fig. 5.

The need for the treble boost (τ_7) was determined during the analysis and will be illustrated later. The values of τ_3, τ_5, and τ_6 were adjusted during the optimization process.

Parameter Optimization

In performing the optimization, two factors were traded off: the position error and a figure of merit representing the noise at threshold. The figure of merit (FOM) was defined as

$$\text{FOM} = \frac{\sqrt{\text{NEB}}}{V_p \, dV/dt}$$

An average FOM for the two directions of scan was used in plotting the data. Many runs were made to iterate the final results. Illustrated in Fig. 6 are the effects of varying individual parameters, while the others are held constant.

The value of 1 Hz for lower cutoff frequency was chosen because little was gained in going lower and the difficulty in supressing $1/f$ noise was increasing. The upper frequency, 400 Hz, was chosen because of its minimum. This minimum being at 400 Hz demonstrates the need for the treble boost circuit to compensate for the 80 Hz thermistor bolometer. The time delay, again, gave minimum return when shorter than the 0.3 m/s value was chosen. A smaller value would have been more difficult to control. From Fig. 6 it can be seen how the choosing of $G = 1.6$ was a compromise with a decision to pick the knee of the curve for minimum drift sensitivity. This resulted in a nominal worst-case error of 0.024 deg with a noise equivalent angle of 0.0068 deg.

To test the sensor analytically over its extreme conditions, the above parameters were varied to limits to account for temperature, aging, etc. The limits established are given in Table 2.

Typical sensor analog outputs are shown in Figs. 7, 8a, and 8b. The July 16, 1970 radiance profile is a worst-case established after looking at many extreme days of data over a several year period. The response to this profile is considered "3 sigma" data and is used as such.

A nominal seasonal variation was run based on a model using 5-yr averages of pressure and temperature. The results of this analysis are shown in Fig. 9.

A summary of cases run covering extreme parameter drifts, seasonal inputs, and altitude and attitude conditions is shown in Table 3. For the maximum and minimum bandwidths, it was assumed all of the components drifted to cause the worst conditions. As can be seen, the worst condition is only 0.03 deg errors; all other cases would be less than this value.

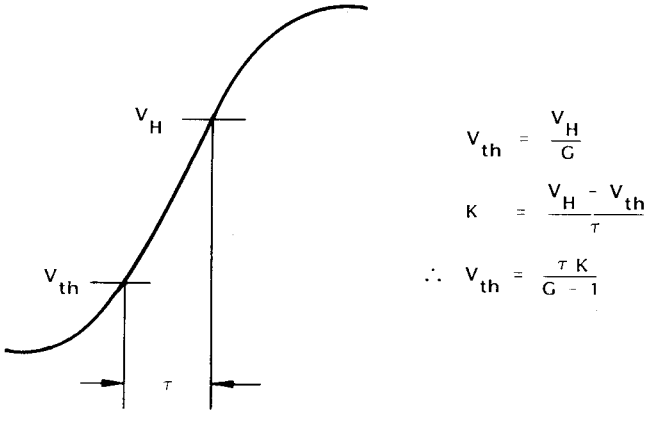

Fig. 4 Slope-sensitive threshold.

Table 1 Comparison of thresholding techniques

Technique	Maximum error, deg
Fixed threshold, space-Earth and Earth-space crossings	0.28
% of peak, space-Earth and Earth-space crossings	0.25
Slope sensitive, space-Earth and Earth-space crossings	0.10
Slope sensitive, space-Earth crossings only	0.03

Table 2 Transfer function parameter errors (ms)

Parameter	Nominal	Error, %	Maximum	Minimum
τ_D	2.0	± 6	2.12	1.88
τ_1	0.10	±20	0.08	0.12
τ_2	5100.0	±32	6732.0	3468.0
τ_3	0.40	±20	0.32	0.48
τ_4	3300.0	±26	4158.0	2442.0
τ_5	0.40	±20	0.32	0.48
τ_6	160.0	±20	192.0	128.0
τ_7	0.50	± 6	0.47	0.53

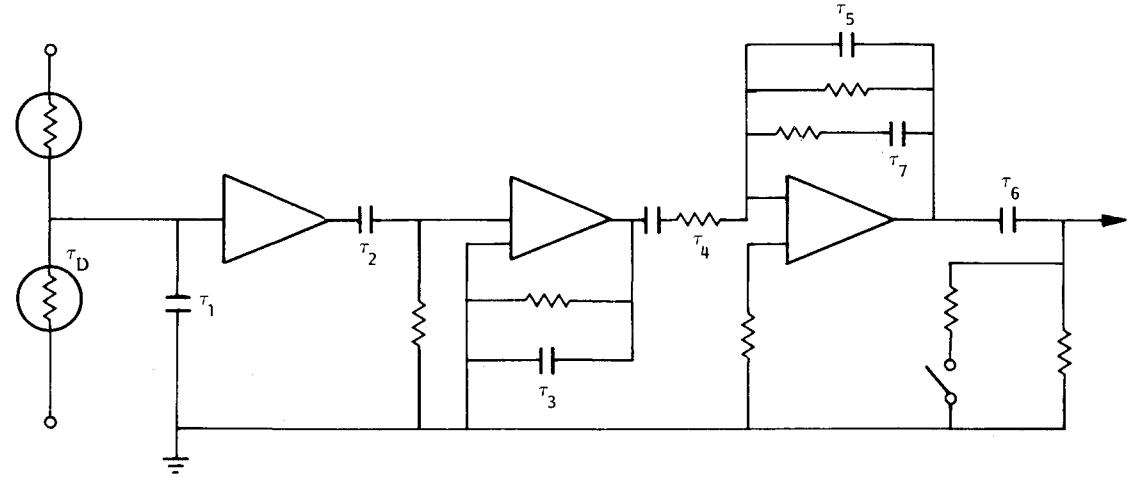

Fig. 5 Sensor transfer function.

Table 3 Analytical results

CASE	RADIANCE MODEL	ALT (NM)	ROLL (DEG)	PITCH (DEG)	BANDWIDTH	G	(MSEC)	ROLL ERROR (DEG)	NOISE (DEG RMS)
1	UNIFORM	19,320	0	0	NOM	1.6	0.30	0.000	0.0057
2	JULY 16, 1970	19,320	0	0	MIN	1.6	0.30	-0.026	0.0070
3	JULY 16, 1970	19,320	0	0	MAX	1.6	0.30	-0.0322	0.0067
4	JULY 16, 1970	19,320	0	0	NOM	1.6	0.362	-0.030	0.0059
5	JULY 16, 1970	19,320	0	0	NOM	1.6	0.238	-0.013	0.0084
6	JULY 16, 1970	19,320	0	0	NOM	1.606	0.30	-0.024	0.0068
7	JULY 16, 1970	19,320	0	0	NOM	1.594	0.30	-0.024	0.0068
8	JULY 16, 1970	19,320	0	0	NOM	1.6	0.30	-0.024	0.0068
9	JULY 16, 1970	19,320	0	6	NOM	1.6	0.30	-0.016	0.0077
10	JULY 16, 1970	14,500	15.8	0	NOM	1.6	0.30	-0.003	0.0039
11	JULY 16, 1970	24,000	12.5	0	NOM	1.6	0.30	-0.011	0.0070
12	JAN 21, 1971	19,320	0	0	NOM	1.6	0.30	0.017	0.0052
13	FEB 12, 1971	19,320	0	0	NOM	1.6	0.30	0.021	0.0063
14	MAR 17, 1971	19,320	0	0	NOM	1.6	0.30	0.004	0.0057
15	APR 18, 1971	19,320	0	0	NOM	1.6	0.30	-0.022	0.0061
16	MAY 22, 1971	19,320	0	0	NOM	1.6	0.30	-0.020	0.0063
17	JUNE 23, 1971	19,320	0	0	NOM	1.6	0.30	-0.027	0.0065

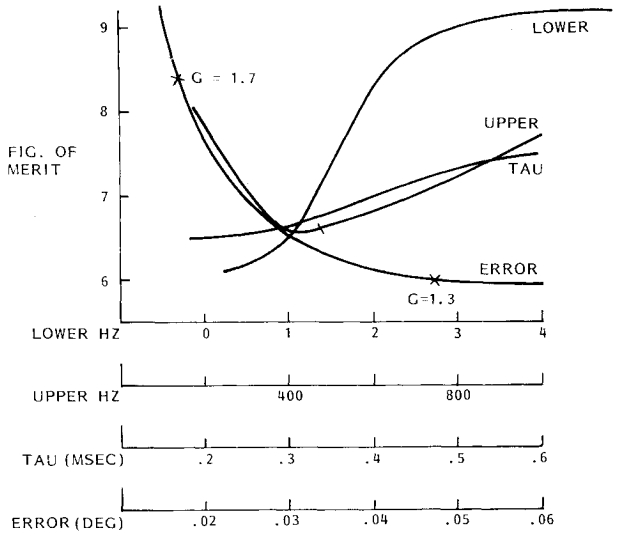

Fig. 6 Figure of merit vs circuit parameters.

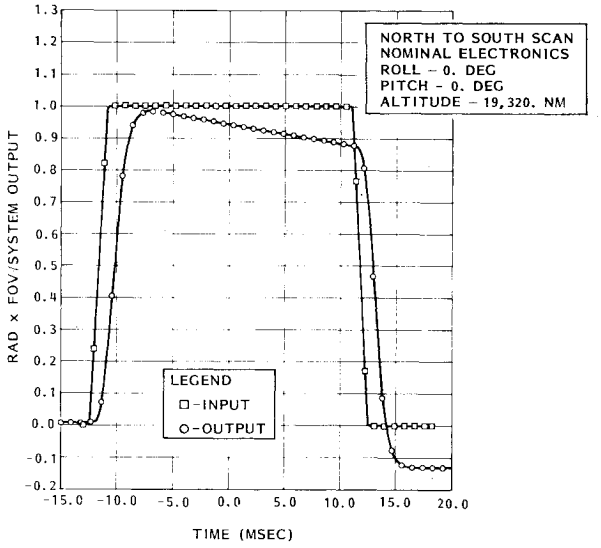

Fig. 7 Uniform Earth radiance.

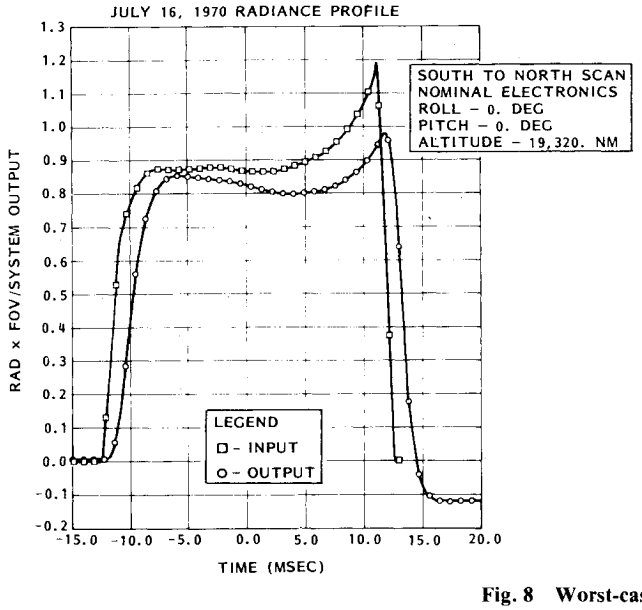

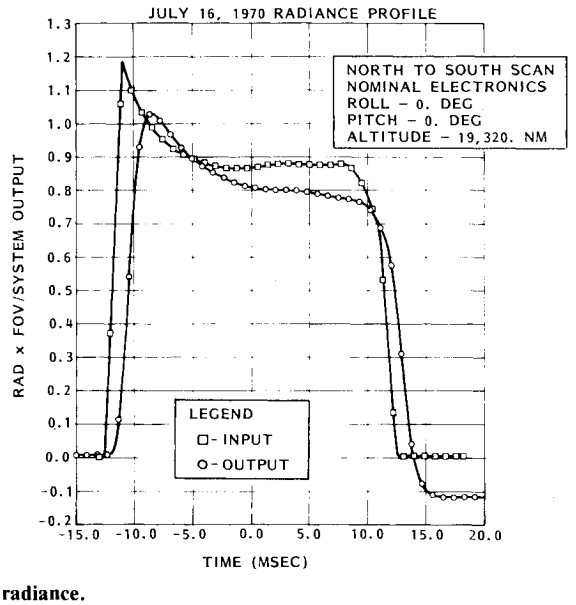

Fig. 8 Worst-case radiance.

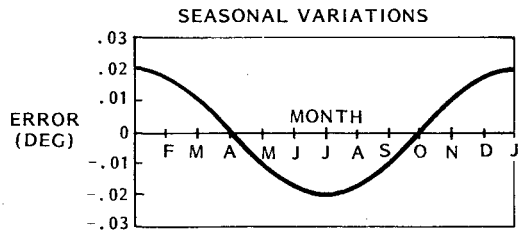

Fig. 9 Nominal seasonal variation.

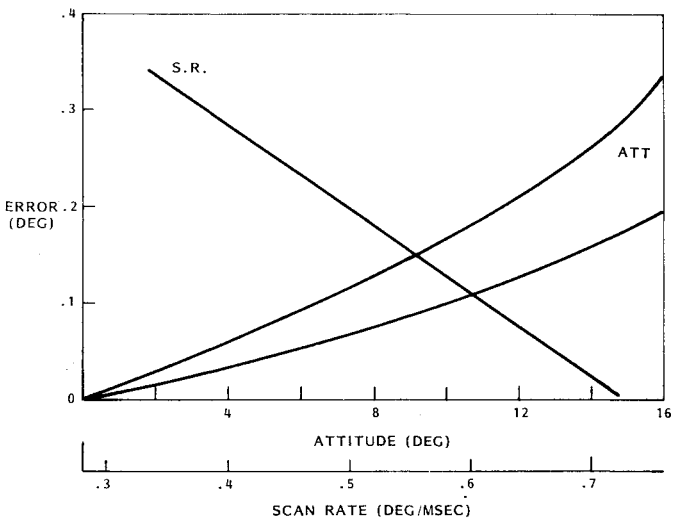

Fig. 10 Error vs attitude, uncompensated scan rate.

Scan Speed Compensation

The slope-sensitive threshold circuit provides a signal which always occurs at the same time after initiation of the signal. For any low pass RC filter, there is a time delay of the output relative to the input which is equal to the slope of the filter phase characteristic. With the circuit parameters chosen, the delay is about 1.6 m/s. This satisfactorily compensates for all radiance effects; however, it causes angular errors as the scan rate at one horizon differs from the scan rate at the opposite horizon, as illustrated in Fig. 10.

In studying the problem further, it was determined that the above error was strictly a function of the difference in scan rates as shown in Fig. 10. To solve this problem, a scan rate compensation count was added. The count at threshold was doubled for 1.6 m/s. When the scan rate at one horizon was more than the opposite horizon, extra counts were added which compensated for the error. The analytical results showing the effect of the compensation on several cases is shown in Fig. 11.

Actual sensor test data confirmed these results. The sensor output is linear to 16 deg within 0.01 deg for various simulated altitudes and cross-axis offsets. The worst-case

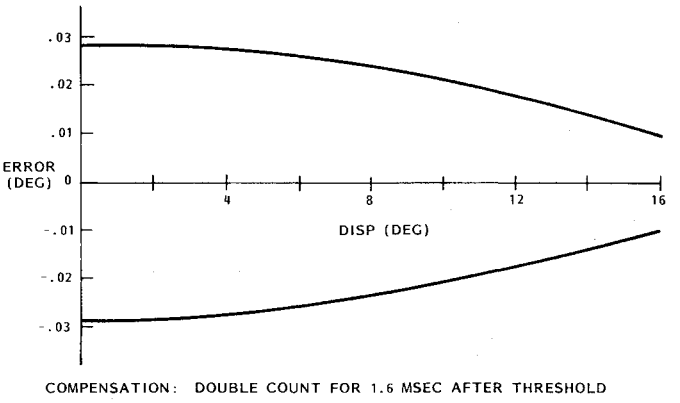

Fig. 11 Error vs attitude, compensated scan rate.

radiance gradient was also simulated with an offset of 0.025 deg occurring as compared to a uniform Earth.

Conclusions

From the analyses performed, verified by test data, the following conclusions can be drawn:

1) The best thresholding technique is an adaptive slope-sensitive circuit using space-Earth crossings only.

2) The optimum bandwidth includes treble boost to increase the high-frequency response of the sensor.

3) The computational algorithm must include compensation for slope changes at the horizon caused by the scanning system.

The above conclusions are applicable to low-altitude horizon sensor design as well as the synchronous orbit system described here. Preliminary analyses indicate similar accuracies are achievable, although no optimizations have been performed to date. The choice of the spectral interval for the sensor, combined with thresholding near the horizon, has made all "cold cloud" errors negligible.

References

[1] Anderson, R.H., "An Advanced Horizon Sensor for Synchronous Altitude 3-axis Stabilized Satellites," *Communication Satellites for the 70's: Technology,* MIT Press, Cambridge, Mass., 1970, pp. 171-187.

[2] Barnett, J.J. et al., "The First Year of the Selective Chopper Radiometer on Nimbus 4," *Quarterly Journal of the Royal Meteorological Society,* Vol. 98, 1972, pp. 17-37.

[3] Barnett, J.J., "The Mean Meridional Temperature Behavior of the Stratosphere from November 1970 to November 1971 Derived from Measurements by the Selective Chopper Radiometer on Nimbus IV," *Quarterly Journal of Royal Meteorological Society,* Vol. 100, 1974, pp. 505-530.

[4] *Global Stratospheric Analysis,* Oxford University, 1972.

[5] Smith, O.E., McMurray, W.M., and Crutcher, H.L., "Cross Sections of Temperature, Pressure, and Density Near the 80th Meridian West," NASA TN D-1641, 1963.

[6] Groves, G.V., "Atmospheric Structure and its Variations in the Region from 25 to 120 km," AFCRL-71-0410, 1971.